I

Publication I

A. Lankinen, T. Tuomi, J. Riikonen, L. Knuuttila, H. Lipsanen, M. Sopanen, A. Danilewsky, P.J. McNally, L. O'Reilly, Y. Zhilyaev, L. Fedorov, H. Sipilä, S. Vaijärvi, R. Simon, D. Lumb and A. Owens, *Synchrotron X-ray topographic study of dislocations and stacking faults in InAs*, Journal of Crystal Growth **283** (2005) 320–327.

Available online at www.sciencedirect.com
SCIENCE DIRECT®
Journal of Crystal Growth 283 (2005) 320–327
JOURNAL OF CRYSTAL GROWTH
www.elsevier.com/locate/jcrysgro

Synchrotron X-ray topographic study of dislocations and stacking faults in InAs

A. Lankinen[a,*], T. Tuomi[a], J. Riikonen[a], L. Knuuttila[a], H. Lipsanen[a], M. Sopanen[a], A. Danilewsky[b], P.J. McNally[c], L. O'Reilly[c], Y. Zhilyaev[d], L. Fedorov[d], H. Sipilä[e], S. Vaijärvi[e], R. Simon[f], D. Lumb[g], A. Owens[g]

[a]*Optoelectronics Laboratory, Helsinki University of Technology, P.O. Box 3500, FIN-02015 TKK, Finland*
[b]*Kristallographisches Institut, Universität Freiburg, D-79104 Freiburg, Germany*
[c]*Research Institute for Networks and Communications Engineering (RINCE), Dublin City University, Dublin 9, Ireland*
[d]*A.F. Ioffe Physico-Technical Institute, St Petersburg 194021 Russia*
[e]*Oxford Instruments Analytical Oy, P.O. Box 85, FI-02631 Espoo, Finland*
[f]*ANKA, Institute for Synchrotron Radiation, Forschungszentrum Karlsruhe, Germany*
[g]*Science Payload and Advanced Concepts Office, ESA/ESTEC, 2200 AG, Noordwijk, The Netherlands*

Received 1 October 2004; received in revised form 15 March 2005; accepted 10 June 2005
Available online 20 July 2005
Communicated by M.S. Goorsky

Abstract

X-ray diffraction topographs made with synchrotron radiation of an epitaxial InAs structure show images of dislocations and stacking faults. Three types of dislocations are identified and their Burgers vectors are determined from a number of topographs having different diffraction vectors and recorded on the same film at a time. Straight dislocations are found to be edge dislocations and their Burgers vector is $\langle 1\,1\,0\rangle$. Also mixed dislocations are found. The overall dislocation density is about $2000\,cm^{-2}$. Large stacking faults are limited by long straight dislocations, the Burgers vector of which is $\langle 1\,1\,0\rangle$. Only a few threading dislocations are observed in the epitaxial layer grown by vapour-phase epitaxy. Their density is about $500\,cm^{-2}$. Small circular dots found are interpreted as indium-rich inclusions.

PACS: 81.05.Ea; 61.72.Ff; 81.10.Bk

Keywords: A1. Crystal defects; A1. X-ray topography; A3. Chloride vapor-phase epitaxy; B2. Semiconducting indium compounds; B3. X-ray detectors

*Corresponding author. Tel.: +35894513120; fax: +35894513128.
E-mail address: Aapo.Lankinen@hut.fi (A. Lankinen).

0022-0248/$ - see front matter © 2005 Elsevier B.V. All rights reserved.
doi:10.1016/j.jcrysgro.2005.06.009

1. Introduction

Indium arsenide is a semiconductor having a direct room-temperature bandgap of 0.35 eV and an electron mobility as large as $33\,000\,cm^2\,V^{-1}\,s^{-1}$ [1]. These properties make it an interesting and useful material for infrared diode lasers and photodetectors. Because InAs strongly absorbs not only infrared radiation but also X-rays, it is a semiconductor with potential similar to GaAs for the development of p–i–n diodes for detectors in the X-ray spectral range of photon energies. Optimal detector performance should be achieved by fabricating devices on a nearly perfect and pure intrinsic InAs wafer and then by growing the doped epitaxial layers on the substrate as defect free as possible. The results of this work will serve as a quality assessment of the InAs wafers after the epitaxial growth process, especially for X-ray detector applications. Particular attention is paid to samples consisting of rather thick layers grown by open tube chloride hydride vapour-phase epitaxy (HVPE) from indium, arsenic chloride and solid arsenic using hydrogen as a carrier gas on InAs substrates acquired from commercial and other sources.

X-ray diffraction topography using synchrotron radiation is a non-destructive technique ideally suited for studying extended defects in electronic materials by imaging the defects and analysing the image contrast [2]. Because of the strong X-ray absorption of III–V semiconductors like InP and GaAs, synchrotron X-ray topography has turned out to be the only practical means of getting a large number of transmission topographs in reasonable exposure times on the same high-resolution film [3–7]. This imaging technique also allowed the determination of the Burgers vector and resulted, e.g. in finding straight screw and mixed dislocations in InP [3] and similar straight dislocations in GaAs [5–7] all possessing a Burgers vector along $\langle 1\,1\,0\rangle$.

InAs has been studied in an earlier work with synchrotron X-ray topography using the transmission geometry [8]. In Ref. [8] the main interest was in the evaluation of the heterostructure consisting of an $In_{0.97}Ga_{0.03}As$ layer grown by liquid-phase epitaxy on an InAs substrate rather than in the characterisation of the defects in the bulk. The InGaAs/InAs structure was intended for use in an infrared detector working in the wavelength range from 1.8 to 5 μm. Two mutually perpendicular sets of misfit dislocations along $\langle 1\,1\,0\rangle$ were observed. The n-type InAs substrate of the InGaAs/InAs heterostructure had a rather uniform and dense dislocation network close to the upper detection limit of about 10^4 dislocations/cm^2 at which individual dislocation images can be discerned in the X-ray diffraction topographs.

2. Experimental procedures

The X-ray diffraction topographs were made at the Topo Beamline at the ANKA (Angstroemquelle Karlsruhe) synchrotron radiation facility in Karlsruhe and at HASYLAB-DESY (Hamburger Synchrotronstrahlungslabor am Deutschen Elektronen-Synchrotron) in Hamburg. Topographs were made on 100×100 mm Slavich VPR-M high-resolution films both in the transmission and in the back-reflection geometry. At ANKA the film-to-sample distance was as long as 70–85 mm whereas at HASYLAB-DESY it was 30–70 mm. At the ANKA topography station the source of radiation is a bending magnet. At HASYLAB-DESY most of the topographs were made at the topography F1 beam line using the radiation of the DORIS bending magnet source having a continuous spectrum of wavelengths. The other source at HASYLAB-DESY was an X-ray undulator of the BW1 beamline. The undulator was tuned to emit a rather narrow spectrum whose maximum occurs at a photon energy of about 10 keV. This was achieved by adjusting the undulator magnet gap and by using two grazing incidence gold-coated silicon mirrors downstream of the beam.

The storage ring of the ANKA facility had an electron momentum of 2.5 GeV/c and a typical beam current of 100–160 mA. The positron ring at DORIS III had a particle momentum of 4.445 GeV/c and a beam current of 80–130 mA. Due to the large particle momentum of the DORIS positron ring compared to the ANKA electron ring the spectrum of radiation extended to

larger photon energies at HASYLAB F1 than at ANKA.

The InAs samples investigated in this work were grown at A. F. Ioffe Physico-Technical Institute using HVPE [9]. The substrate was a (0 0 1) oriented Czochralski-grown n+ -type wafer having an electron concentration of $10^{17}\,cm^{-3}$. The substrate temperature in epitaxial growth was about 750 °C, and the HVPE reactor high-temperature zone was at 800 °C. The epitaxial layer had a thickness of 40 μm and an electron concentration of $(2-9)\times 10^{16}\,cm^{-3}$ at room temperature. The sample thickness, including the epilayer, was 360 μm. Another sample was grown on a 4° toward ⟨1 1 1⟩ misoriented (0 0 1) substrate having a rather large electron concentration of $2\times 10^{18}\,cm^{-3}$. The epitaxial layer on this sample had a thickness of 10 μm and an electron concentration of $10^{17}\,cm^{-3}$.

The (0 0 1) surfaces of the sample wafers were set perpendicular to the incident beam or in certain cases at a tilt angle of 14°−18° measured from the vertical [1 1 0] direction.

3. Burgers vector analysis

An analysis of the Burgers vectors of dislocations is possible with the aid of the topograhic images of the dislocations. The type of the dislocation can be resolved if both the Burgers vector $\vec{b}$ of the dislocation and the direction vector $\vec{l}$ of the dislocation line are known [10]. If $\vec{b}$ and $\vec{l}$ are parallel, the dislocation is a pure screw dislocation. If $\vec{b}$ and $\vec{l}$ are perpendicular to each other, the dislocation is an edge dislocation. Quite frequently $\vec{b}$ and $\vec{l}$ are neither parallel nor mutually perpendicular and the dislocation is called a mixed dislocation.

The image of a dislocation disappears in an X-ray topograph, if

$$\vec{g}\cdot\vec{b}=0, \tag{1}$$

where $\vec{g}$ is the diffraction vector $[h\,k\,l]$. Upon the identification of at least two topographs, in which the dislocation is not visible, $\vec{b}$ can be solved by using Eq. (1). Consequently, a mixed dislocation never completely disappears in any topograph.

It is often difficult to find the direction $\vec{l}$ of the dislocation. One could assume that the dislocation goes through the sample from the front to the back surface. By knowing the thickness of the sample and the length of the image in a given topograph the direction $\vec{l}$ can be calculated. Another way to find $\vec{l}$ is to determine it from stereo pair topographs. Any two topographs recorded on the same film form such a pair. Sometimes, as in the case of an edge dislocation, it is not necessary to know the exact direction of the dislocation. It is sufficient to determine whether $\vec{b}$ is perpendicular to $\vec{l}$.

4. Results and discussion

4.1. Dislocations

Fig. 1 shows four transmission topographs of the InAs sample, enlarged from the same film. The product of the linear absorption coefficient μ and the sample thickness t is $\mu t \approx 6.6$, 6.6, 5.6 and 8.4 for the reflections $\bar{3}\bar{3}1$, $\bar{3}31$, $\bar{6}02$, and 331, respectively. Because all these values of μt are significantly larger than unity, anomalous transmission occurs and dynamical images of dislocations are seen. They appear as white lines against the perfect crystal background. The white dislocation lines that are marked with dashed ovals are visible in the $\bar{3}31$ and $\bar{6}02$ topographs and disappear in the $\bar{3}\bar{3}1$ and 331 topographs. Applying Eq. (1) a straightforward calculation gives the result that the Burgers vector $\vec{b}$ of these dislocations is parallel to $[1\,\bar{1}\,0]$.

The sample was oriented so that $[1\,\bar{1}\,0]$ points to the right in Fig. 1. Therefore, the white marked dislocation lines are perpendicular to $[1\,\bar{1}\,0]$ and consequently they are edge dislocations. It is worth noting that similar edge dislocations whose Burgers vectors were aligned to ⟨1 1 0⟩ were observed in undoped GaAs grown by the vapour pressure controlled Czochralski (VCz) method [7], suggesting that these two III–V materials have common properties in their dislocation structures. However, the relationship between the different growth techniques and the effect of substrate doping need further research efforts.

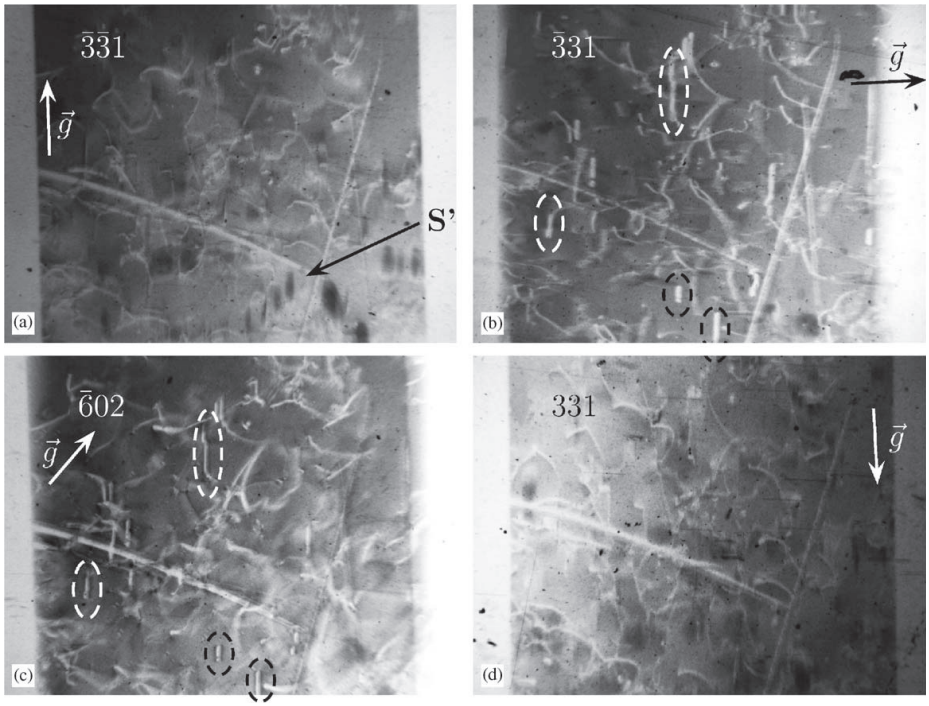

Fig. 1. (a) $\bar{3}\bar{3}1$, (b) $\bar{3}31$, (c) $\bar{6}02$, and (d) 331 synchrotron transmission topographs of InAs. Image width is 2 mm. Dislocation images are marked with arrows and dashed ovals. **S′** marks a stacking fault. Diffraction vector projections are marked with $\vec{g}$.

Fig. 2 shows a stereo pair of $\bar{1}\bar{5}1$ and $1\bar{5}1$ transmission topographs. These two topographs were enlarged from the same film as those presented in Fig. 1. In Fig. 2 $\bar{1}\bar{5}1$ and $1\bar{5}1$ reflections had $\mu t \approx 2.8$, which implies that both kinematical and dynamical images can co-exist. The dislocation images of Fig. 2 consist predominantly of black lines indicating a kinematical image contrast, but the dynamical images can also be seen, albeit very faintly. The white images of Fig. 1 are dynamical images of the same dislocations. In addition to the linear edge dislocations in both Figs. 1 and 2 there are circular arc dislocations. Analogous to similar dislocations in GaAs [6,7] they are identified as mixed dislocations, the Burgers vectors of which are along $\langle 1\,0\,1\rangle$. The proportion of the circular arc dislocations is larger in semi-insulating GaAs grown by VGF than in slightly doped InAs studied in this work. The overall dislocation density of the sample is about 2000 cm^{-2}, which is slightly more than the density of 1500 cm^{-2} found in VGF and VCz GaAs [6,7]. About half of the dislocations are circular arc dislocations. The exact number of circular arc dislocations is not clear, because some of the linear dislocation images might actually be arc dislocations seen from the plane they lie in. Due to the different growth techniques commonly used in fabricating substrates of these III–V materials, it is not clear whether the differences in the dislocation structures and densities are material based or growth related.

Fig. 3 shows the $1\bar{1}7$ back-reflection topograph of the epitaxial-layer side of the same region of the

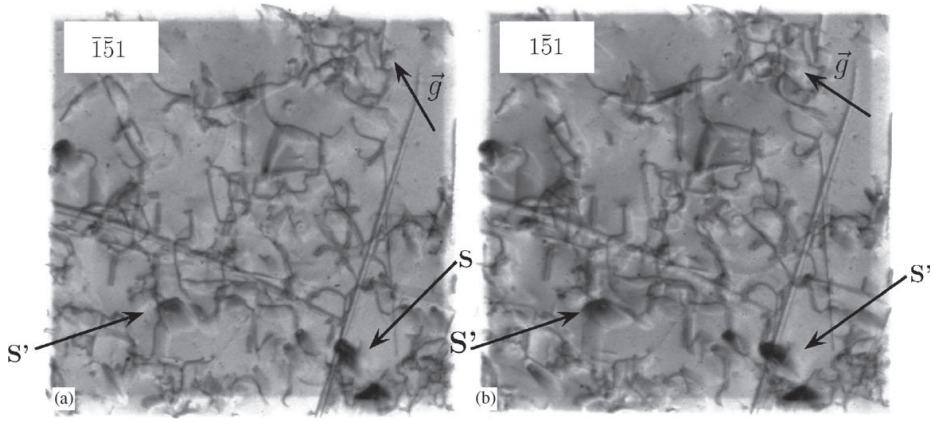

Fig. 2. Stereo pair of (a) $\bar{1}\bar{5}1$ and (b) $1\bar{5}1$ transmission topographs of InAs. Image width is 2 mm. Stacking faults **S′** are marked with arrows and diffraction vector projections with $\vec{g}$.

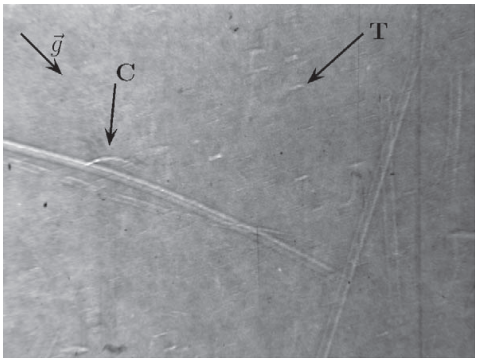

Fig. 3. $1\bar{1}7$ back reflection topograph from epitaxial layer side of InAs. **T** marks a threading dislocation, **C** marks a circular arc dislocation and $\vec{g}$ the projection of the diffraction vector. Image width is 2 mm.

sample as shown in the transmission topographs of Figs. 1 and 2. The X-ray attenuation length is 9, 79 and 58 μm for the contributing reflections $1\bar{1}7$, $3\bar{3}21$ and $4\bar{4}28$, respectively, which implies that the image is mainly from the epitaxial layer of the sample. The short, nearly horizontal, parallel and predominantly white lines are interpreted as the ends of threading dislocations, one of which is marked with **T**. The dislocation density of the epilayer is about $500\,\mathrm{cm}^{-2}$, which is clearly less than the overall dislocation density of the whole sample. This shows that most of the dislocations present in the substrate do not penetrate into the epitaxial layer. Because Fig. 3 shows only one clearly visible circular arc dislocation image, marked with **C**, most of the circular arc dislocations are confined into the substrate. Thus, the epilayer threading dislocations originate likely from the linear substrate dislocations. The open tube HVPE grown epitaxial InAs layer had fewer dislocations than the InAs substrate it was grown on, indicating that the HVPE growth method can be used to grow thick epitaxial layers with low dislocation density on InAs, which is of importance for the fabrication of the p–i–n X-ray detector structures.

The topographs of Figs. 1–3 are from the epitaxial structure that had the smallest density of defects. For comparison, Fig. 4 shows a $\bar{2}\bar{2}8$ back-reflection topograph of the other epitaxial sample grown on a substrate having a large electron concentration of about $2 \times 10^{18}\,\mathrm{cm}^{-3}$. This topograph displays a clear misfit dislocation network at the interface between the intrinsic InAs epitaxial layer and the heavily doped substrate. Topographs of an intrinsic epitaxial layer on the

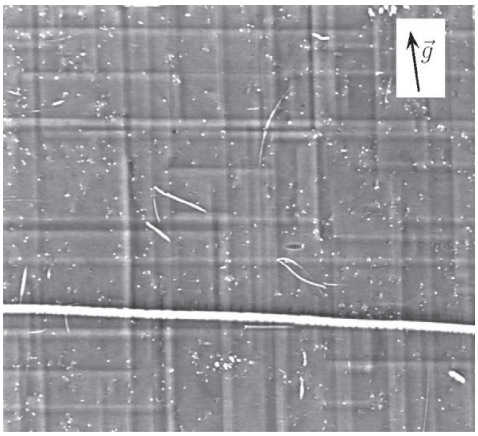

Fig. 4. $\bar{2}\bar{2}8$ back reflection topograph of an InAs epitaxial layer grown on heavily doped InAs substrate showing misfit dislocations in the interface. The broad white horizontal line is an image of a scratch on the sample surface. Diffraction vector projection is marked with $\vec{g}$. Image width is 2 mm.

less doped (about 10^{17} cm^{-3}) substrate in Fig. 3 did not show any signs of misfit dislocations. In addition, rather a large number of small (10 μm in diameter) white dots are clearly visible in Fig. 4. These dots are believed to be ends of threading dislocations having density of about 25 000 cm^{-2}, which is approximately 50 times as large as that of the best sample.

Fig. 5 shows four transmission topographs of the same sample as the topographs of Figs. 1 and 2, but taken at a different location on the wafer. Straight and circular arc dislocations similar to those in Figs. 1 and 2 are also seen in Fig. 5. In the middle of the topographs of Fig. 5 there are images of small dislocation loops marked with **L**. They are located on the (0 0 1) plane, which is parallel to the sample surface.

4.2. Stacking faults

In addition to the dislocations discussed in Section 4.1, Fig. 5 shows rather large grey areas marked with **S** and **S′**. These areas are identified as images of stacking faults. The images of the stacking faults are darker (thus having larger diffracted intensity) than the background, because a new wavefield generated by the crossing field at the fault boundary adds intensity to the diffracted beam [11]. The image contrast of the stacking faults of type **S′** and **S** is especially strong in the 511 topograph of Fig. 5(a) and $\bar{1}51$ topograph of Fig. 5(d), respectively. Two stacking faults on the right-hand side of the topographs marked with **S** are limited by long straight parallel lines. These four lines are interpreted as partial dislocations and the enclosed grey areas as stacking faults. The partial dislocations on the left-hand sides of the stacking faults disappear in the $\bar{1}51$ topograph. Their Burgers vector is most likely ⟨1 0 1⟩.

The round stacking faults **S′** have a more complicated structure. These kind of stacking faults are seen in all topographs of this work. For example, in Fig. 1 they are very common and in some areas they line up in a row as observed in the $\bar{3}\bar{3}1$ topograph of Fig. 1. Other good examples of stacking faults like **S′** may be observed in Fig. 2. The peripheries of the **S′** stacking fault images seem to be formed by straight dislocations, the Burgers vector of which are along ⟨1 1 0⟩.

4.3. Precipitates

Fig. 6 shows a 004 transmission topograph of the same sample as in Figs. 1–3 and 5, but imaging yet another area of the sample. Apart from the dislocation lines the most striking features in this topograph are the small circular dots clearly visible in the two enlargements. The black and white contrast of such dots, one of which is marked with **P** in the left enlargement suggests the presence of a precipitate or a void. Because the contrast of the dots is black on the positive side of the $\vec{g}$ vector, the black–white dots originate from precipitates that compress the surrounding lattice [12,13]. Precipitates in bulk III–V semiconductors are commonly predicted to consist of the group V elements, i.e. in this case of arsenic, similar to the well-studied GaAs precipitation [14,15]. According to the dynamical theory of X-ray diffraction the precipitates seen in the topographs are close to the surface [12,13].

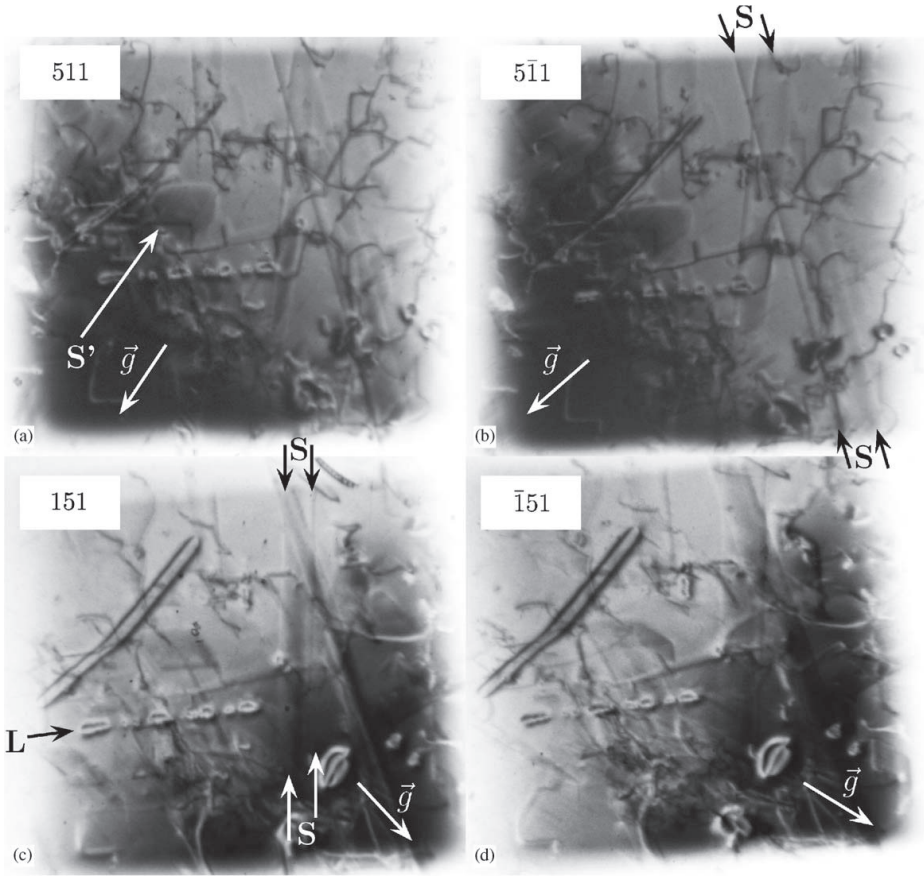

Fig. 5. 511, $5\bar{1}1$, 151 and $\bar{1}51$ transmission topographs of InAs. Image width is 1.5 mm. Stacking faults **S** and **S′**, dislocation loops **L** and diffraction vector projections $\vec{g}$ are marked with arrows.

5. Conclusion

Edge dislocations having a Burgers vector $\vec{b}$ parallel to $\langle 1\,1\,0\rangle$ are found in InAs epitaxial samples grown by vapour-phase epitaxy. The dislocations lie in the 1 1 0 plane perpendicular to $\vec{b}$. In addition to these straight edge dislocations, circular arc dislocations are observed in synchrotron transmission X-ray topographs. The circular arc dislocations are similar to those found frequently in vertical gradient freeze grown and vapour pressure Czochralski grown GaAs crystals. They are identified as mixed dislocations, which have the same Burgers vector $\vec{b}$ parallel to $\langle 1\,1\,0\rangle$ as the straight ones.

Stacking faults as well as precipitates are also common defects in InAs. The rather thick undoped epitaxial layer grown on the n-type substrate having an electron concentration of $10^{17}\,\mathrm{cm}^{-3}$ is well lattice matched. The back-

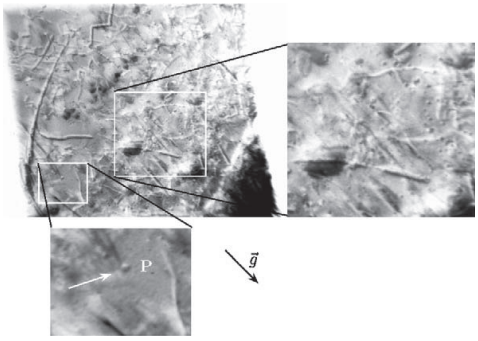

Fig. 6. 004 transmission topograph of InAs. Image width is 2 mm. **P** indicates a precipitate. Diffraction vector projection is marked with $\vec{g}$.

reflection topographs show only a few images of threading dislocations on the (0 0 1) sample surface.

The crystalline quality of the InAs i–n structure grown by vapour-phase epitaxy in this work is almost as good as the similar GaAs i–n structure grown by the same technique [6]. Although the stacking faults and precipitates may cause problems it is believed that InAs p–i–n diodes are potentially useful device structures. The diodes are viable candidates for development as X-ray detectors and further investigations are required to determine whether their performance is better than that exhibited by similar GaAs devices [16].

Acknowledgements

This work was supported by the European Space Agency Contract 17356/03/NL/CP and by the IHP-Contract HPRI-CT-2001-00140 of the European Commission.

References

[1] O. Madelung (Ed.), Data in Science and Technology, Semiconductors Group IV Elements and III–V Compounds, Springer, Berlin, 1991, pp. 133–141.
[2] T. Tuomi, J. Synchrotron Radiat. 9 (2002) 174.
[3] K. Naukkarinen, T. Tuomi, V.-M. Airaksinen, K.-M. Laakso, J.A. Lahtinen, J. Crystal Growth 64 (1983) 485.
[4] T. Tuomi, H. Lipsanen, T. Ranta-aho, J. Partanen, J.A. Lahtinen, E. Monberg, R.A. Logan, J. Crystal Growth 96 (1989) 881.
[5] E. Prieur, T. Tuomi, J. Partanen, E. Yli-Juuti, M. Tilli, J. Crystal Growth 132 (1993) 599.
[6] T. Tuomi, M. Juvonen, R. Rantamäki, K. Hjelt, M. Bavdaz, S. Nenonen, M.-A. Gagliardi, P.J. McNally, A.N. Danilewsky, E. Prieur, M. Taskinen, M. Tuominen, Mat. Res. Soc. Symp. Proc. 487 (1998) 459.
[7] T. Tuomi, L. Knuuttila, J. Riikonen, P.J. McNally, W.-M. Chen, J. Kanatharana, M. Neubert, P. Rudolph, J. Crystal Growth 237–239 (2002) 350.
[8] P.J. McNally, J. Curley, A. Krier, Y. Mao, J. Richardson, T. Tuomi, M. Taskinen, R. Rantamäki, E. Prieur, A. Danilewsky, Semicond. Sci. Technol. 13 (1998) 345.
[9] M.J. Cardwell, J. Crystal Growth 70 (1984) 97.
[10] D.K. Bowen, Exercises in diffraction contrast, in: B.K. Tanner, D.K. Bowen (Eds.), Characterization of Crystal Growth Defects by X-Ray Methods, Plenum Press, New York, 1980, Ch. A3, pp. 528–534.
[11] J. Chikawa, Laboratory techniques for transmission X-ray topography, in: B.K. Tanner, D.K. Bowen (Eds.), Characterization of Crystal Growth Defects by X-Ray Methods, Plenum Press, New York, 1980, Ch. 15, pp. 368–400.
[12] T. Tuomi, R. Rantamäki, P.J. McNally, D. Lowney, A.N. Danilewsky, P. Becker, J. Phys. D 34 (2001) A133–A135.
[13] B.K. Tanner, X-ray Diffraction Topography, Pergamon, Oxford, 1976, pp. 71–77.
[14] A.G. Cullis, P.D. Augustus, D.J. Stirland, J. Appl. Phys. 51 (1980) 2556.
[15] P. Schlossmacher, K. Urban, H. Rüfer, J. Appl. Phys. 71 (1992) 620.
[16] A. Owens, M. Bavdaz, A. Peacock, A. Poelaert, H. Andersson, S. Nenonen, H. Sipilä, L. Tröger, G. Bertucci, J. Appl. Phys. 90 (10) (2001) 5376.